Textures of surfactant monolayers

Thomas M. Fischer,[1,*] Robijn F. Bruinsma,[2] and Charles M. Knobler[1]
[1]*Department of Chemistry and Biochemistry, University of California, Los Angeles, California 90024*
[2]*Department of Physics, University of California, Los Angeles, California 90024*
(Received 10 December 1993)

Microscopy studies of coexistence droplets of (tilted) surfactant molecules absorbed at air-water interfaces have demonstrated that such droplets contain a variety of textures. In this paper we describe the observed droplet textures using the Landau free energy for tilted hexatic surfactant films, supplemented by a boundary energy. It is shown that this free energy can naturally explain the morphology of droplet textures with sixfold symmetry. In particular, it predicts (i) the existence of a continuous transition from straight to kinked domain walls and (ii) the appearance of spiral textures associated with spontaneous chiral symmetry breaking in part of the phase diagram. We compare the predicted textures with recent polarized fluorescence and Brewster-angle microscopy experiments.

PACS number(s): 68.10.−m, 64.70.Md, 61.30.Jf, 68.15.+e

I. INTRODUCTION

A. Surfactant monolayers

Surfactant molecules form monomolecular films at air-water interfaces. If the molecules are insoluble in water such films are called Langmuir monolayers while monomolecular films of soluble amphiphiles are known as Gibbs monolayers. These monolayers are important for both biological and technical reasons. For example, lungs will not function without the coating of a surfactant monolayer; monolayers transferred from water to solid supports are the basis of chemical and biological sensors. Surfactant monolayers are also of fundamental physical interest, however, because they allow investigation of naturally occurring two-dimensional ($D=2$) systems which are relatively easy to prepare. It is well known that the statistical mechanics of $D=2$ many-body systems often is quite different from that of three-dimensional ($D=3$) systems. A well-known example of unusual physics in $D=2$—and relevant for what follows—is the prediction by Nelson and Halperin [1] of the existence of the so-called "hexatic" phase as a new phase intervening between $D=2$ liquids and solids. Hexatics are, in essence, $D=2$ liquid crystals that lack translational order but retain order in the orientations of the bonds between the center-of-mass positions of neighboring molecules. The bond-orientational order leads to a sixfold orientational symmetry in the phase. Hexatic phases are not common, but they have been encountered in free-standing smectic (Sm) liquid crystal films [2].

In recent years, phase diagrams of Langmuir monolayers have been investigated in considerable detail [3]. Macroscopic studies, such as isotherm measurements in which the $D=2$ pressure is determined as a function of the monolayer area, have been supplemented by microscopic methods, such as surface x-ray diffraction studies, which have revealed the nature of the monolayer phases. The phase diagram of monolayers exhibits the $D=2$ analogs of the usual gas, liquid, and solid phases of $D=3$ materials, but additional phases are found as well. In particular, one encounters a variety of higher density "liquid-condensed" (LC) phases, which intervene between the solid and a low-density "liquid-expanded" (LE) phase.

The existence of a multiplicity of phases in Langmuir monolayers should not really be surprising. Surfactant molecules consist of nonpolar hydrocarbon tails (generally 25–40 Å in length) attached to hydrophilic polar head groups. At area densities typical of those of LC phases, the tails of the surfactant molecules have a rodlike conformation. It is well known that $D=3$ liquids of rodlike molecules can condense into a variety of liquid-crystal mesophases. It is thus natural to suppose that the various LC phases could be $D=2$ analogs of familiar liquid-crystal mesophases, while the LE phase would correspond to the $D=2$ analog of an isotropic liquid (the surfactant tails in the LE phase have a more random conformation). This relationship was proposed at least 60 years ago [4], but it is only recently that the x-ray studies have demonstrated [5] that the molecular packings in surfactant monolayer phases bear a one-to-one correspondence to certain known smectic liquid-crystalline phases [6].

Four of these phases are believed to be hexatics [5]. They differ primarily in the orientation of their tails with respect to the surface normal and the bond-orientational order. In the discussion by Bibo, Knobler, and Peterson [3] they have been classified as the LS ("superliquid"), L_1', L_2, and L_2^* phases. A very schematic phase diagram is shown in Fig. 1. In the LS phase, the average direction of the tails is perpendicular to the surface while in the remaining phases the tails are tilted. The tail orientation can be described by introducing the position dependent two-component unit vector $\hat{\mathbf{c}}(\mathbf{x})$ (or "c director"), which indicates the projection onto the surface of the average direction of the molecular tails (see Fig. 1, inset). The c

*Present address: Facultät für Physik und Geowissenschaften, Universität Leipzig, Linnestr. 5, D-04103, Leipzig, Germany.

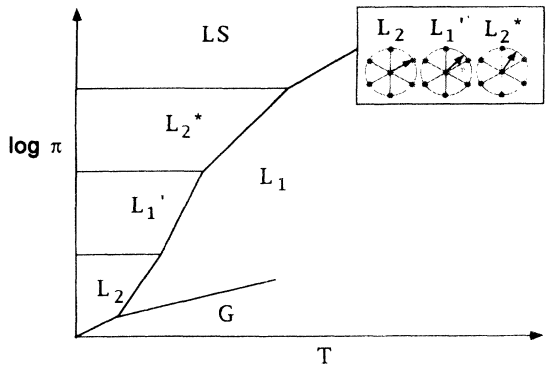

FIG. 1. Schematic pressure-temperature (π-T) phase diagram showing several of the monolayer phases that have been identified in fatty acids and their esters. The relative locations of the gas (G), liquid-expanded (L_1), and superliquid phases (LS) are much the same for many substances. The locations of the other phases and the positions of the boundaries between them are more variable and less well known. The inset shows the orientation of the molecular tilt azimuth with respect to the local sixfold structure of the head groups that exists in the three tilted hexatic phase L_1', L_2, and L_2^*.

director points toward nearest neighbors in the L_2 phase, toward next-nearest neighbors in the L_2^* phase, and along an intermediate direction in the L_1' phase. In the language of smectic liquid crystals, the tilted LC phases are the analogs of, respectively, the smectic-*I*, -*F*, and -*L* phases (we will use this latter notation). The fact that the surfactant liquid crystals appear to be hexatics is somewhat surprising since tilted hexatics are less common in the phase behavior of $D=3$ liquid crystals. On the other hand, the nematic phase, which is quite common in $D=3$ liquid crystals, appears to be absent in the surfactant films studied to date.

Liquid crystals in $D=3$ are birefringent and can be characterized visually by their striking multicolored *textures* when viewed between polarizers; the textures reflect the spatial variation of the local optical axis of the material. This spatial variation may be due to metastable "defects," which for topological reasons cannot decay, or, for finite systems, it may be imposed by boundary conditions at the sample boundary. Textures are also very useful as a quick diagnostic for the type of liquid crystal involved. Recent studies of monolayers by polarized fluorescence [7] and Brewster-angle reflection [8,9] have shown that the spatial variation of the c director can be observed and demonstrated that LC phases of surfactant monolayers also exhibit textures; see Fig. 2.

At first sight, it would appear natural to expect that LC-phase textures should be similar to those of the analogous $D=3$ smectic phases for achiral molecules (the surfactant molecules used were generally achiral). The most striking texture of the $D=3$ phases is a fivefold star-shaped object [2]. The appearance of stars in tilted hexatics can be readily explained by allowing the c director to couple to the local orientation of the six hexatic crystallographic axes (see below). LC phases have indeed been found to exhibit star textures very similar to those of the free-standing tilted smectic hexatic films, but a large variety of other textures has been found as well. For example, the "ground state" of the LC phase for some fatty acids is a stripe texture consisting of straight or kinked defect lines [10]. The mesoscopic studies thus suggest that the analogy between surfactant monolayers and the $D=3$ tilted-hexatic liquid crystals may not be complete since in the latter the ground state is believed to be uniform.

B. Droplet textures

The spatial variation of the optical axis of a texture reflects an inhomogeneous structure of the underlying order parameter. The order parameter of an LC phase is rather complex: it is a combination of the c director and

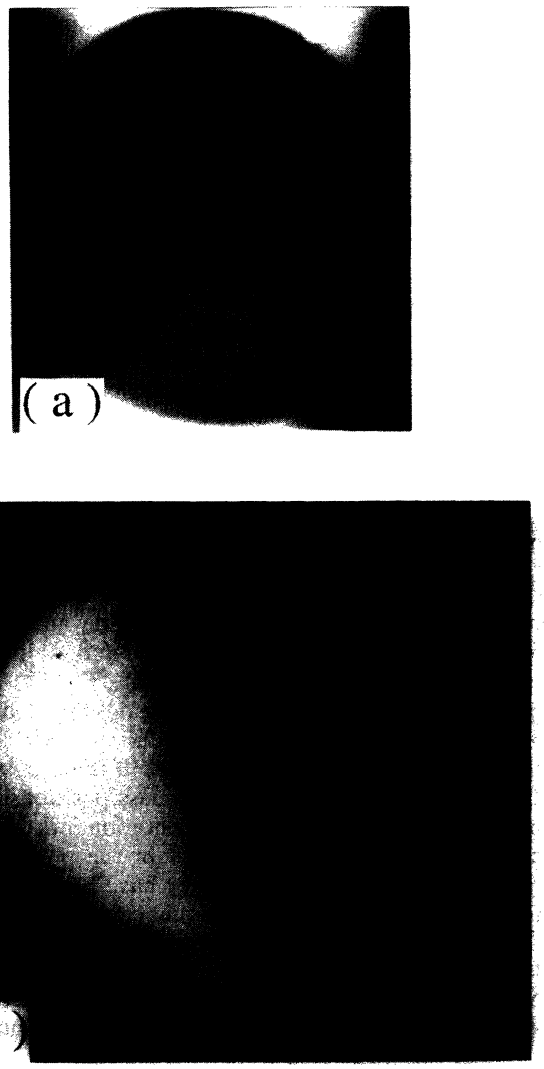

FIG. 2. Images of droplet textures. The droplets are surrounded by the liquid expanded phase, which is isotropic. (a) Polarized fluorescence microscope image of a star defect in a monolayer of methyl octadecanoate. (b) Brewster-angle microscope image of a boojum in a monolayer of pentdecanoic acid (courtesy J. Meunier).

the hexatic order parameter. We characterize the hexatic order by the angle θ made by the six crystallographic axes with a fixed axis, say, the x axis (see Fig. 3). This "bond-angle" field $\theta(\mathbf{x})$ can, like $\hat{\mathbf{c}}(\mathbf{x})$, vary across the sample. Obviously, $\theta(\mathbf{x})$ is defined only modulo 60° so the LC free energy must be invariant under rotations by multiples of 60°. It is the experience in $D=3$ systems that complex order parameters produce complex textural patterns and, as mentioned, a bewildering variety of textures has indeed been observed in monolayers. The question now is whether we can hope to carry out a program of texture classification in surfactant monolayers in the same way as has been done for $D=3$ liquid crystals [11]. In this paper we will address this issue only for the simplest possible case, namely, that of a $D=2$ LC droplet inside a LE matrix. In such a confined geometry, the number of allowed textures should be severely reduced by the boundary constraints imposed on both the $\hat{\mathbf{c}}(\mathbf{x})$ and $\theta(\mathbf{x})$ fields at the LE-LC interface because they raise the energy cost of adding metastable topological defects. Electrostatic repulsions inhibit the coalescence of LC droplets and their sizes are therefore generally only of order 100 μm; their shapes usually vary between circular to (rounded) hexagonal.

Coexistence droplets in ester monolayers show a range of textures; some common ones are shown in Fig. 4. As one moves along the LE-LC coexistence curve, reversible changes are observed in both the texture and the droplet shape. On the basis of these relaxation processes, it is reasonable to assume that the observed textures represent a local equilibrium of the free energy rather than a frozen, or pinned, configuration determined entirely by the preparation history of the drops. The fluorescence data on the esters also reveal that $\hat{\mathbf{c}}(\mathbf{x})$ is fairly strongly anchored along the normal to the LE-LC interface. The boundary condition on the bond-angle field (if any) is not known since the $\theta(\mathbf{x})$ field cannot be visualized by the fluorescence studies. The observed textures are often based on the sixfold hexagonal "basic motif" shown in Fig. 4(a). The origin of the basic motif is easily understood if we assume that the hexatic degree of freedom is

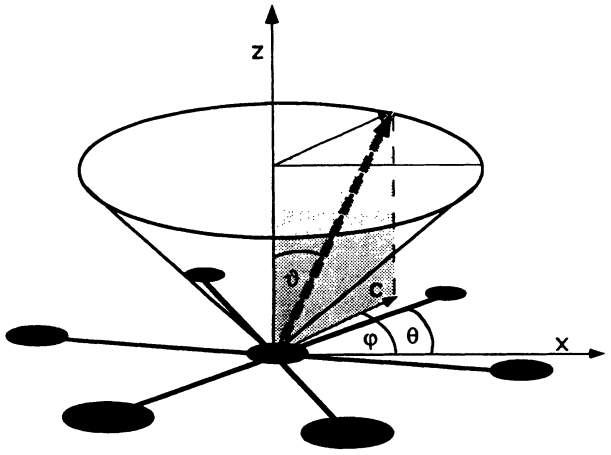

FIG. 3. Definition of the bond angle θ, the tilt angle ϑ, the tilt azimuth φ, and the director c.

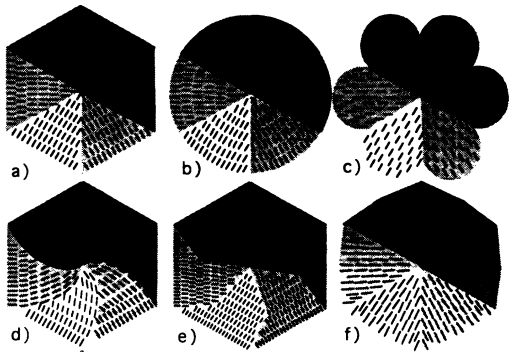

FIG. 4. Droplet textures for hexatic phases. The lines indicate the orientation of the molecular tilt azimuth within each domain and the shading gives an impression of the contrast that would be observed in an image obtained by polarized fluorescence microscopy.

relatively stiff and thus spatially uniform across the drop. In each of the six sectors of the hexagon, the in-plane director is also uniform and locked to the bond-angle field with the relative angle between them assuming the equilibrium value appropriate for the LC phase in question. At the boundary between adjacent sectors, $\hat{\mathbf{c}}(\mathbf{x})$ makes a rapid rotation of 60° to flip from one of the six hexatic directions to the next ("60° wall"). On the other hand, coexistence droplets of fatty acid monolayers have textures with no sharp boundaries but rather a smoothly varying c director. Understanding the origin of the different phenomenology of ester surfactants and fatty acid surfactants is important for learning how to interpret the observed textures.

If the droplet shape is a perfect hexagon, then the basic motif naturally satisfies normal boundary conditions for the c director at the LE-LC interface. In this view, hexagonal droplet shapes would be a consequence of the normal boundary conditions on the molecular tail rather than the direct influence of the hexatic order on the LE-LC interface. This is confirmed by the fact that in the high-pressure LS phase, where the molecules are perpendicular to the air-water interface, the droplets are *not* hexagonal even though the phase is believed to be hexatic [7]. It is important for the following to note that the strength of the boundary conditions on the c director is, in reality, limited. As shown in Fig. 4(b), experiments also show the existence of circular drops with a hexagonal interior structure, which could only satisfy normal boundary conditions by distorting the textural uniformity inside the six sectors, which does not appear to be the case. As will be discussed below, a circular shape is actually a natural variation of the basic motif if we allow for an increase of the LE-LC line tension with respect to that of a 60° wall.

The basic motif is closely related to the five-armed star-shaped defects observed both in the LC phase of materials such as pentadecanoic acid away from the coexistence line as well as in freely suspended films of tilted smectic hexatics. We can crudely think of the basic motif as a stable star-type defect imposed by the LE-LC phase boundary. The difference between the two textures is

that in a true fivefold star, the tilt and bond degrees of freedom necessarily are not uniform inside the star segments whereas for the ideal basic motif they are uniform. Also, the five defect lines of the star terminate at point defects while the six defect lines of the basic motif terminate at the LE-LC phase boundary (it is actually the energy cost of the point defects of a star that controls the number of arms of the star).

Typical droplet shapes and textures of the esters, shown in Figs. 4(a)–4(e), show a variety of variations on the basic motif of Fig. 4(a).

(i) The observed droplet shapes vary from circular to hexagonal [Figs. 4(a) and 4(b)] while rosette-shaped coexistence droplets have been observed [12] as well [see Fig. 4(c)].

(ii) The basic motif is frequently found [7,12] to be deformed into sixfold "spiral" and "broken-spiral" patterns [Figs. 4(d) and 4(e)]. Both left- and right-handed deformations of the spokes of the hexagon are encountered. This chirality provides us with a puzzle since, although chiral textures are encountered in the free-standing tilted hexatic films, it appears to be necessary for the constituent molecules to be chiral while the constituent surfactant molecules used in the Langmuir monolayer experiments showing the spirals are achiral. Note, however, that if we leave the I or the F phase to enter the L phase, we must make a left or right choice. In other words, the L-phase order parameter has broken chiral symmetry even though the constituent molecules are achiral. It is not known at present whether the droplets with spiral textures indeed are in the L phase.

(iii) Less common variations are textures with three defect lines emerging from a point on the LE-LC boundary or textures with defect lines that appear to terminate near the center of the droplet.

Star textures are less common in droplets of fatty acids. A characteristic texture in that case appears to be the "boojum" [see Figs. 2(b) and 5(a)], which has been observed by Brewster-angle microscopy [9,13].

It is the aim of this paper to see whether the basic motif and its variations can be naturally explained with the type of Landau–de Gennes theories [11] that have been very successful in explaining the textures in $D=3$ liquid crystals. A theoretical description of textures in surfactant monolayers must be based on a model coupling the two order-parameter fields (i.e., the c-director and bond-angle fields). Such a theory was previously developed by Nelson and Halperin [14] for the case of liquid-crystal films of tilted hexatics, which have the same order-parameter structure as hexatic surfactant films. Selinger and Nelson [15] discussed the resulting I-L-F phase diagram and showed that the model can describe the star textures observed by Dierker, Pindak, and Meyer [2] in free-standing films of tilted hexatics. However, the ground state of the model is always uniform and no spiral textures are encountered, so it cannot be directly applied to surfactant films. Selinger *et al.* [16] proposed that this originates from the fact that the Landau free energy of a surfactant monolayer (i) does not need to be reflection invariant with respect to mirror reflection in the plane of the film and (ii) does not need to obey any $c \rightarrow -c$ symmetry because of the head-tail asymmetry of surfactant molecules located at an interface. This lowering of the symmetry—an example of surface ferroelectricity [17]—combined with the intrinsic head-tail asymmetry of the surfactant molecules allows new terms in the free energy. Because of such terms, the ground state of surfactant monolayers need not be translationally invariant. For example, for sufficiently strong head-tail asymmetry the ground state of the I and F phases is an array of parallel 60° splay-type defect lines where the tails (or heads) have an unusually high concentration, somewhat resembling a $D=2$ variant of the well known L_α phase of surfactant molecules in $D=3$ [18]. (In the L phase, it also possible to have a stripe pattern with alternating chirality and bend deformation in the texture.) The stripe textures observed in fatty acids [10,13,19] indeed appear to be consistent with an array of splay walls. We will, in the following, supplement the free energy of Selinger *et al.* [16] with an expression for the LE-LC boundary energy to see whether the model is also able to reproduce the observed droplet textures.

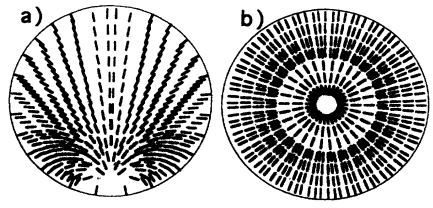

FIG. 5. Droplet textures without domain walls. (a) $m=1$ boojum splay defect; (b) $m=1$ splay defect.

II. CONTINUUM THEORY

In this section, we will develop the continuum theory that will form the basis of a subsequent discussion of textures. We start by briefly reviewing the Landau free energy for hexatic surfactant monolayers as proposed in Refs. [14–16]. A Landau free energy of Langmuir monolayers in an LC phase should describe (i) the relative free energy cost of the I, L, and F phases and (ii) the free energy cost of spatial variations of the tilt and bond-angle fields. We will restrict ourselves to the case of monolayers with tilted molecules. The c director will be denoted by

$$\hat{\mathbf{c}}(\mathbf{x})=\cos\varphi(\mathbf{x}),\sin\varphi(\mathbf{x}) \tag{2.1}$$

with $\varphi(\mathbf{x})$ the tilt-azimuth field of the molecular tails (see Fig. 3). We will always assume that the polar angle between the molecular tails and the surface normal is fixed at some equilibrium value by local molecular interactions. The reason that we can neglect spatial variations of the polar angle is that a global simultaneous rotation over any angle of the azimuthal angle $\varphi(\mathbf{x})$ and the bond-angle field $\theta(\mathbf{x})$ is a symmetry operation of the system as a whole and thus should cost no energy (neglecting boundary effects). A corresponding coupled long-wavelength spatial variation of the two fields thus should cost relatively little energy. On the other hand, the polar

angle has no such "gapless mode" and any variation away from its equilibrium value will be energetically costly. If we restrict ourselves to low-energy textures, we can thus neglect variations of the polar angle.

The simplest possible Landau free energy per unit area f consistent with the symmetries of a tilted hexatic surfactant monolayer is

$$f=\tfrac{1}{2}K_6(\nabla\theta)^2+\tfrac{1}{2}K_1(\nabla\cdot\hat{\mathbf{c}})^2+\tfrac{1}{2}K_3(\nabla\times\hat{\mathbf{c}})+V[6(\theta-\varphi)] -\lambda_s\cos[6(\theta-\varphi)]\nabla\cdot\hat{\mathbf{c}}-\lambda_b\sin[6(\theta-\varphi)]z\cdot(\nabla\times\hat{\mathbf{c}}) . \tag{2.2}$$

The first term in f is the deformation energy of a nonuniform $D=2$ hexatic with K_6 the hexatic rigidity; this term describes the energy cost of spatial variations in the bond-angle field. The magnitude of K_6 is not known, but if K_6 is large compared to K_1 and K_3 (see below), then thermodynamic stability of the hexatic phase requires that K_6 exceed k_BT_c (times a numerical constant of order one) with k_B the Boltzmann constant and T_c the transition temperature between the hexatic and the isotropic liquid (the LE phase in the present case). The second and third terms in Eq. (2.2) represent the usual deformation free energy of a $D=2$ nematic liquid crystal. There are two Frank constants: the splay rigidity K_1 and the bending rigidity K_3, both, like K_6, having the dimensions of energy. Not much is known about their magnitudes except that they must be less than K_6 for the case of the esters.

The fourth term is the coupling energy between the two fields. The function $V(\theta-\varphi)$ is periodic in $\theta-\varphi$ with period $2\pi/6$. This ensures both the sixfold periodicity of the bond-angle field as well as the invariance under simultaneous global rotations of the bond-angle and tilt-azimuth fields. Following Selinger and Nelson [15], we expand the coupling in a Fourier series. The first two terms are

$$V\approx -h_6\cos[6(\theta-\varphi)]-h_{12}\cos[12(\theta-\varphi)]-\cdots . \tag{2.3}$$

The minimum of V determines the nature of the phase. In terms of the relative angle $\theta-\varphi$, there are three possibilities [assuming that we can keep only the two terms of Eq. (2.3)]: (i) For $h_6>0$ and $h_6>-4h_{12}$, the minimum is at $\theta-\varphi=m2\pi/6$, with $m=0,1,\ldots,5$ (I phase). (ii) For $h_6<0$ and $h_6<4h_{12}$, the minimum is at $\theta-\varphi=\pi/6+m2\pi/6$ (F phase). (iii) For $-4h_{12}>h_6>4h_{12}$ and $h_{12}<0$, there are 12 minima at $\theta-\varphi=\pm\alpha+m(2\pi/6)$, with α an angle intermediate between 0 and $\pi/6$ (L phase). The sign in front of α determines whether the phase has right- or left-handed chirality.

As a function of h_6 there is, for positive h_{12}, a sharp first-order transition at $h_6=0$ from the I to the F phase, while for negative h_{12} there are two second-order transitions at $h_6=\pm4h_{12}$ (see Fig. 6). The L phase intervenes between these two limits with α varying from zero at the I-L phase boundary to $\pi/6$ at the L-F phase boundary.

The last two terms in the free-energy density require special discussion. They are permitted for surfactant monolayers (but not for bulk systems) because of (i) the asymmetry between the air and water media at whose interface the surfactant molecules are located and (ii) the head-tail asymmetry of surfactant molecules. The divergence of the c director represents a splay of the texture. Because of the head-tail asymmetry, splayed textures with $\hat{\mathbf{c}}(\mathbf{x})$ replaced by $-\hat{\mathbf{c}}(\mathbf{x})$ must have a different energy. Since $\nabla\cdot\hat{\mathbf{c}}$ is a scalar under the symmetry operations of all three phases, terms linear in $\nabla\cdot\hat{\mathbf{c}}$ are in principle allowed. However, $\nabla\cdot\hat{\mathbf{c}}$ by itself is a total derivative, which can be adsorbed in the boundary conditions discussed below. The splay term thus can only contribute to the free-energy density if we multiply it by a position-dependent scalar. To construct such a scalar out of the φ and θ fields, we define the two unit vectors $\hat{\mathbf{d}}=(\cos6\varphi,\sin6\varphi)$ and $\hat{\mathbf{e}}=(\cos6\theta,\sin6\theta)$. The lowest-order scalar consistent with the sixfold symmetry is $\hat{\mathbf{d}}\cdot\hat{\mathbf{e}}$ and $(\hat{\mathbf{d}}\cdot\hat{\mathbf{e}})\nabla\cdot\hat{\mathbf{c}}$ produces the λ_s term in f. The parameter λ_s [which has units of (energy)/(length)] is a measure of the head-tail asymmetry of the surfactant molecules residing at the interface.

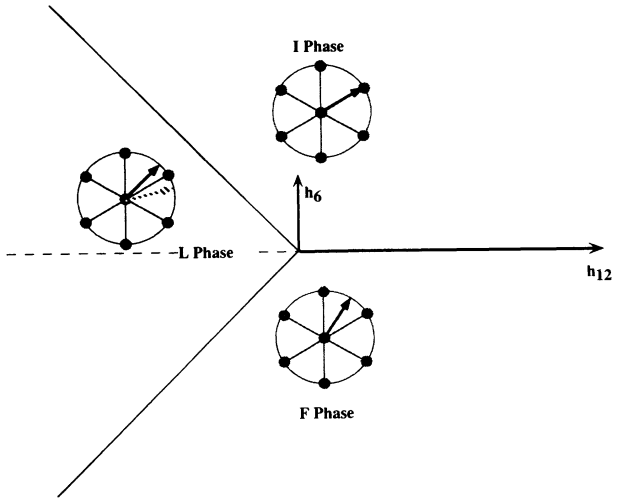

FIG. 6. Phase diagram of tilted hexatic monolayers as a function of the potential parameters h_6 and h_{12}. The insets show the orientation of the tilt azimuth with respect to the bond angle in each phase.

The pseudovector $\nabla\times\hat{\mathbf{c}}$ represents a bend of the texture. Since there is no reflection symmetry at the air-water interface, a term of the form $\hat{\mathbf{z}}\cdot\nabla\times\hat{\mathbf{c}}$, with $\hat{\mathbf{z}}$ the interface normal, would seem possible, but it is in fact not permitted in the Landau free-energy density because it transforms as a *pseudoscalar*. We can, however, construct a scalar from the dot product of $\nabla\times\hat{\mathbf{c}}$ with $\hat{\mathbf{d}}\times\hat{\mathbf{e}}$, which provides the λ_b term in Eq. (2.2). Note that this scalar vanishes if θ is locked to ϕ at the two equilibrium angles (0 and 30°) corresponding to the I and F phases [see discussion following Eq. (2.3)] so it plays a role only in the chiral L phase. We can define

$$X\equiv\langle\sin[6(\theta-\varphi)]\rangle \tag{2.4}$$

as a chiral order parameter, which is nonzero only in the L phase. It couples linearly to the bend of the texture according to Eq. (2.2).

We now must construct a Landau-type expression for the interfacial energy between the liquid-condensed and the liquid-expanded phases. If we want to compare textural energies of coexistence droplets, such a term must be added to the area contribution (i.e., the integral of f over the droplet area). This interfacial energy must depend on the relative orientation between the normal to the LE-LC boundary $\hat{\mathbf{n}}$, the c director, and the hexatic axes. We will assume that the lock-in energy has an analytic dependence on the relative angle β between the c director and $\hat{\mathbf{n}}$ so that it can be expanded in a Fourier series in β in the same spirit as Eq. (2.3). For the reasons given in the Introduction, we will assume that the hexatic degree of freedom does not couple to the interfacial energy.

There is again no head-tail symmetry at the LE-LC interface and thus no $c \rightarrow -c$ symmetry. This means that the Fourier series must start directly with the $\cos(\beta)$ and $\sin(\beta)$ terms. The lowest-order terms in the Fourier series of the interfacial energy F_i are then

$$F_i \approx \oint ds \{ \gamma - \Gamma_1 \hat{\mathbf{c}} \cdot \hat{\mathbf{n}} - \Gamma_2 [2(\hat{\mathbf{c}} \cdot \hat{\mathbf{n}})^2 - 1] - \cdots \} . \tag{2.5}$$

The first term in Eq. (2.5) is the isotropic LE-LC interfacial line tension γ. The second term corresponds to the $\cos(\beta)$ contribution. The $\sin(\beta)$ term is proportional to $\hat{\mathbf{z}} \cdot \nabla \times \hat{\mathbf{c}}$. Since such terms are forbidden in the I and F phases and since Eq. (2.5) must hold in all three phases, we are not allowed to include it. The sign of the constant Γ_1 distinguishes whether the tail or the head prefers to be normal to the boundary. The third term is the $\cos(2\beta)$ contribution, which would be the lowest-order boundary term for nematic liquid crystals (which do obey the $c \rightarrow -c$ symmetry). Thermodynamic stability of the LE-LC interface requires that the interfacial energy as a whole be positive.

We will assume that the Fourier series converges sufficiently fast that we can restrict ourselves to the first few terms discussed above. The optimal boundary angle β as a function of Γ_1 and Γ_2 is then easily found by minimizing Eq. (2.5): (i) For Γ_1 positive and $\Gamma_1 > -4T_2$, $\beta = 0$. (ii) For Γ_1 negative and $\Gamma_1 < 4\Gamma_2$, $\beta = \pi$. (iii) $\cos(\beta) = -\Gamma_1 / 4\Gamma_2$ in the remaining case.

If Γ_2 is positive, the boundary energy is thus always minimal if the c director is normal to the boundary (with Γ_1 determining whether the head or tail sticks out of the droplet). For negative Γ_2, the optimal orientation for the c director is either again along the normal or at an angle β with the normal that varies continuously from 0 to π if $|\Gamma_1| < 4|\Gamma_2|$. We conclude that, in contrast to the case of $D = 3$ nematics, where parallel boundary conditions are common, parallel boundary conditions are not realized in surfactant monolayers at LE-LC interfaces except for the special case when Γ_1 is exactly zero. Since Γ_1 is in general permitted to be finite, we should not expect to encounter parallel boundary conditions in the LC phases except for a special line in the phase diagram defined by $\Gamma_1(\Pi, T) = 0$. Normal boundary conditions are expected to be most commonly encountered. Most (but not all) textures examined indeed appear to have normal boundary conditions. We will assume that Γ_1 is large compared to Γ_2, so we always have a preferred normal orientation. Physically, this is reasonable because the molecular tails of the surfactant molecules at the interface are likely to prefer, for entropic reasons, the lower-density environment of the liquid-expanded phase. Thermodynamic stability then imposes $|\Gamma_1| < \gamma$; otherwise we could create negative interfacial energies by a suitable orientation of the c director with respect to the interface normal.

The boundary conditions on the c director in the L phase must be considered separately. Returning to the bulk free energy Eq. (2.2), the Gauss and Stokes theorems state that

$$\int d^2 r \, \nabla \cdot \hat{\mathbf{c}} = \oint ds \, \hat{\mathbf{c}} \cdot \hat{\mathbf{n}} , \tag{2.6a}$$

$$\int d^2 r \, \hat{\mathbf{z}} \cdot \nabla \times \hat{\mathbf{c}} = \oint \hat{\mathbf{z}} \cdot \hat{\mathbf{n}} \times \hat{\mathbf{c}} . \tag{2.6b}$$

If θ is everywhere strictly locked to φ, then, from Eq. (2.6a), $\lambda_s \cos[6(\theta - \varphi)]$ reduces to a trivial renormalization of Γ_1 while the $\lambda_b \sin[6(\theta - \varphi)]$ term produces a "$\sin(\beta)$" type contribution to the boundary energy. This contribution is proportional to the (pseudoscalar) chiral order parameter X, so it only appears in the L phase, as it should. If one assumes λ_b to be small compared to the Γ parameters, then the textural boundary conditions of the locked L phase are found to be

$$\beta \approx \frac{\lambda_b X}{\Gamma_1 + 4\Gamma_2} \tag{2.7a}$$

(i) for Γ_1 positive and $\Gamma_1 > -4\Gamma_2$,

$$\beta \approx \pi + \frac{\lambda_b X}{\Gamma_1 + 4\Gamma_2} \tag{2.7b}$$

(ii) for Γ_1 negative and $\Gamma_1 < 4\Gamma_2$, and (iii)

$$\cos(\beta) = -\Gamma_1 / 4\Gamma_2 \tag{2.7c}$$

in the remaining case. We thus conclude that in the L phase, in regions where the c director is locked to the hexatic axes, the molecular tails cannot be strictly normal to LE-LC interface and that their angle is proportional to the chiral order parameter.

An important ingredient in the discussion of alternative textures is the characteristic length scales that can be constructed by combining the various parameters in the free energy. We start with the λ_s splay term, which is linear in $\nabla \cdot \hat{\mathbf{c}}$. It favors inhomogeneous splay-type textures while the restoring elastic terms, which favor a homogeneous texture, are quadratic in $\nabla \cdot \hat{\mathbf{c}}$. This means that in general the free energy can be lowered by allowing a splay texture with a characteristic length scale:

$$\xi_s = K_6 / \lambda_s , \tag{2.8a}$$

assuming the rigidity K_6 against deforming the hexatic degree of freedom to be greater than the splay and bend Frank constants. If the sample is large compared to ξ_s, we expect to encounter a deformed splay texture in the ground state, while for sample sizes small compared to this length, the ground-state deformation would be small.

Similarly, the characteristic length for a bend modulation is

$$\xi_b = K_6/\lambda_b \ . \tag{2.8b}$$

Selinger *et al.* [16] found that ξ_s and ξ_b are the characteristic length scales of the stripe patterns decorating the ground state of the LC phase in the case of infinite films. If we identify the stripe texture observed experimentally in the LC phase away from coexistence with the predicted stripe patterns, then these length scales are of order 100 μm. This is somewhat larger than the typical size of the coexistence droplets, so the textural deformation produced by the λ_s and λ_b terms in the free energy should be modest. We thus will treat the two terms using perturbation theory.

By combining the Frank energies with the coupling $V(\theta-\varphi)$ between the hexatic and orientational degrees of freedom, we can identify more characteristic length scales. The two most relevant ones are

$$\zeta_6 = \sqrt{K_1/h_6} \ , \tag{2.9a}$$

$$\zeta_{12} = \sqrt{K_1/h_{12}} \ . \tag{2.9b}$$

The physical meaning of these two length scales is that of "healing lengths": they determine how rapidly the relative angle $\theta-\varphi$ will approach the equilibrium value appropriate to the phase in question if this angle has been perturbed away from equilibrium at some point. Tilted LC phases generally contain many defect lines where the molecular tail flips from one azimuthal orientation to another (see Sec. IV) and their width should be set by these healing lengths. The widths of these defect lines as determined by Brewster-angle microscopy [9] indicate that healing lengths are about 2–3 μm.

III. LOCKED TEXTURES

We begin our discussion of textures by assuming that the lock-in energy $V(\theta-\varphi)$ between the hexatic and orientational degrees of freedom is sufficiently large so that the relative angle $\theta-\varphi$ can be kept fixed at an equilibrium value appropriate to the phase under consideration. We will discuss later the condition for locked textures to be realized. Experimentally, the condition appears to hold for the case of LE-LC coexistence droplets of fatty acids. The assumption of lock-in simplifies the full free energy F (i.e., the integral of f over the droplet area plus the LE-LC boundary energy) to $F=F_B+F_S$ with

$$F_B = \int dx\, dy \{ \tfrac{1}{2}(K_1+K_6)(\nabla\cdot\mathbf{c})^2 + \tfrac{1}{2}(K_3+K_6)(\nabla\times\mathbf{c})^2 \} \ , \tag{3.1a}$$

$$F_S \approx \gamma \oint ds - \bar{\Gamma}_1 \oint ds\, \hat{\mathbf{c}}\cdot\hat{\mathbf{n}} - \bar{\lambda}_b \oint ds\, \hat{\mathbf{z}}\cdot\hat{\mathbf{c}}\times\hat{\mathbf{n}} - \Gamma_2 \oint ds [2(\hat{\mathbf{c}}\cdot\hat{\mathbf{n}})^2 - 1] \ , \tag{3.1b}$$

where

$$\bar{\Gamma}_1 = \Gamma_1 + \lambda_s \cos[6(\theta-\varphi)_{\rm eq}] \ , \tag{3.2a}$$

$$\bar{\lambda}_b = \lambda_b \sin[6(\theta-\varphi)_{\rm eq}] \ . \tag{3.2b}$$

Note that $\bar{\lambda}_b$ is proportional to the chiral order parameter X. The bulk term F_B is the free energy of a $D=2$ nematic with an effective splay Frank constant K_1+K_6 and an effective bend constant K_3+K_6. The only metastable defects of a $D=2$ nematic are point defects called disclinations. They can be classified, just as for $D=3$ nematics, by the rotation of the director on going around the defect in a closed circuit. If $\Delta\alpha$ is the rotation angle of $\hat{\mathbf{c}}$ around the defect, then we must demand that $\Delta\alpha = m2\pi$, with m an integer. Half-integer disclinations, which are present in $D=3$ nematics, are forbidden here because $\hat{\mathbf{c}}$ and $-\hat{\mathbf{c}}$ correspond to physically distinct molecular orientations. An $m=1$ point disclination obeying normal boundary conditions is shown in Fig. 5(b) ($m=-1$ disclinations are inconsistent with normal boundary conditions in a circular drop [11] and will be ignored).

To construct a textural pattern, we must first minimize F with respect to the tilt-azimuth angle φ. This produces a complex nonlinear equation that simplifies greatly if we set the two Frank constants equal:

$$\Delta\varphi = 0 \ , \tag{3.3}$$

i.e., the tilt-azimuth angle obeys the Laplace equation. Nevertheless, we shall see that it is important to allow K_1 and K_3 to differ. Accordingly, we will assume that the general nature of textures for which K_1 and K_3 are *not* equal is similar to that of the solutions of Eq. (3.3) and use those solutions to construct trial textures whose variational parameters are found by minimizing the full free energy.

We start with a pure $m=1$ splay point defect at the center of the coordinate system. This texture has a c director that is parallel (or antiparallel) to the radial unit vector (we will choose the orientation that minimizes the boundary energy). This indeed is a solution of Eq. (3.3) (with the tilt-azimuth angle φ equal to the in-plane azimuth angle). The free energy cost of an $m=1$ splay defect in a circular drop of radius R is then

$$F = 2\pi \ln(R/a_0)[K_1+K_6] + 2\pi R(\gamma - |\bar{\Gamma}_1| - \Gamma_2) + E_c(m=1) \ , \tag{3.4}$$

where a_0 is a cutoff (of molecular size). The constant $E_c(m=1)$ describes the disclination core energy, i.e., the contribution to ΔF from a core region with a radius of order the molecular length a_0, where our continuum theory would not be valid. A circular droplet with no texture at all would have an energy of $F=2\pi\gamma R$. An $m=1$ disclination has a lower energy than such a uniform drop provided the droplet radius exceeds a length of order $E_c(m=1)/|\Gamma_1|$ or $(K_1+K_6)/|\Gamma_1|$, whichever is larger.

We can also have point defects that are mixtures of splay and bend. An obvious trial state is another (and more general) solution of Eq. (3.3)

$$\hat{\mathbf{c}}_l = \cos(\phi+\varphi_0), \sin(\phi+\varphi_0) \ , \tag{3.5}$$

with $\varphi=\phi+\varphi_0$, ϕ the in-plane azimuthal angle, and φ_0 a variational parameter. The "field lines" of this texture are, for general φ_0, logarithmic spirals with φ_0 controlling

the pitch. If φ_0 is zero or π, the texture reduces to a pure $m=1$ splay disclination and if φ_0 is $\pm\pi/2$, to a pure bend disclination. The pitch angle of the trial texture is equal to the boundary angle β of the c director with the LC-LE interface normal discussed in Sec. II. The trial free energy is

$$F=2\pi\ln(R/a_0)[K_6+K_1\cos^2(\varphi_0)+K_3\sin^2(\varphi_0)]$$
$$+2\pi R[\gamma-\bar{\Gamma}_1\cos(\varphi_0)-\Gamma_2\cos(2\varphi_0)-\bar{\lambda}_b\sin(\varphi_0)]$$
$$+E_c(m=1)\ , \tag{3.6}$$

where we assume that the core energy does not depend on the pitch of the spiral. Note that the hexatic rigidity does not couple to the pitch angle of the spiral. Minimizing the free energy with respect to the pitch angle φ_0 of the spiral gives results that depend on the droplet radius. Assuming $\bar{\Gamma}_1 \gg \bar{\lambda}_b$, we find the following.

(i) $R \gg K_{1,3}/|\bar{\Gamma}_1|$. In this range of droplet radii, the boundary energy F_s dominates and fixes the pitch angle so φ_0 assumes the value of the boundary angle β computed in Sec. II. Assuming that the preferred boundary orientation of the c director is to be along the interface normal, droplets of the I and F phase should exhibit radial splay textures while those of the L phase should exhibit a spiral texture whose pitch angle is proportional to the chiral order parameter X [see Eqs. (2.7a) and (2.7b)].

(ii) $R \ll K_{1,3}/|\bar{\Gamma}_1|$. In this range, the nematic free energy F_B dominates and the preferred boundary conditions need not be obeyed. We find the following results:

$$\varphi_0 \approx \begin{cases} \bar{\lambda}_b R/(K_3-K_1)\ln(R/a_0)\ , & K_1<K_3 \quad (3.7a) \\ \pi/2+|\bar{\Gamma}_1|R/(K_1-K_3)\ln(R/a_0)\ , & K_1>K_3\ . \quad (3.7b) \end{cases}$$

Since $\bar{\lambda}_b$ is proportional to the chiral order parameter, it follows that for $K_1<K_3$ the texture is radial in the I and F phases and spiral in the L phase [compare Eqs. (2.4) and (3.2b)]. The pitch of the spiral remains a measure of the chiral order parameter [although the proportionality constant differs from the one found in (i)]. For $K_1>K_3$, the texture is nearly pure bend with circular field lines. Combining the two results, we see that in both cases (i) and (ii) the appearance of a spiral texture correlates with being in the L phase, while textures may undergo a dramatic reorganization at the threshold $K_1=K_3$. We will see that these conclusions have more general validity. Although $m=1$ disclinations appear to be natural textures for droplets, they have not been observed in alkyl-ester monolayers.

It was implicit in our variational ansatz that any spiral texture is homogeneous across the drop. This assumption may be invalid if the bulk contribution to the free energy prefers a bend texture while the surface energy demands normal boundary conditions. For $K_1>K_3$ and large R, we should expect to find a spiral texture that resembles an $m=1$ bend texture at the origin and an $m=1$ splay texture at the boundary. This type of texture is not related to the growth of a chiral order parameter, but should be easily distinguishable from the uniform spiral textures discussed previously by the radial gradient in the fluorescence or Brewster intensity. A second assumption embodied in our trial texture is that of azimuthal symmetry. A single point defect that does not have azimuthal symmetry is the so-called "boojum," an $m=1$ splay defect pulled to the edge of the sample [Fig. 5(a)]. If we choose the origin of a polar coordinate system to lie at the droplet edge where the boojum is to be located, then the appropriate solution of Eq. (3.3) is

$$\hat{c}=\cos(2\phi),\sin(2\phi) \tag{3.8}$$

for $r<2R\cos(\varphi)$. The free-energy cost of this texture is (normal boundary conditions)

$$F=2\pi\ln(2R/a_0)[K_6+\tfrac{1}{2}(K_1+K_3)]-0.2[K_1+K_6]$$
$$-0.9[K_3+K_6]+2\pi R(\gamma-|\bar{\Gamma}_1|-\Gamma_2)+E_c(\text{boojum})\ . \tag{3.9}$$

The textural part of the free energy of the boojum is very close to that of an $m=1$ disclination (if the two Frank constants are about equal). It is not possible, however, to compare the respective defect energies because the core energy of a boojum will generally be quite different from that of a disclination because the core of the boojum is located at the LE-LC boundary while the disclination core is deep inside the droplet. A droplet containing a boojum will no longer be circularly symmetric because the asymmetric texture exerts a torque on the LE-LC interface.

If the core energy of the boojum is high compared to the splay energy, it may be more favorable to place the core *outside* the sample as discussed by Langer and Sethna [20] and Hinshaw and Petschek [21] for chiral Sm-C^* films. This avoids the divergent energy at the core and produces a more uniform texture inside the droplet but, for a pure boojum texture, at the cost of a violation of normal boundary conditions. Boojum textures of this type have indeed been observed in Gibbs monolayers of fatty acids by Hénon and Meunier [9] and in Langmuir monolayers of pentadecanoic acid by Overbeck, Hönig, and Möbius [13]. In ester monolayers, boojum-type textures have also been observed, but they contain line defects of the type discussed in Sec. IV.

The boojum textures with a virtual core represent a balance between a violation of the normal boundary conditions and increased textural uniformity. To examine droplet textures for weak boundary conditions more generally, it is convenient to use polynomial solutions of Eq. (3.3):

$$\varphi(x,y)=\varphi_0+ax+by+cxy+d(x^2-y^2)\cdots\ , \tag{3.10}$$

which define a family of second-order curves along which the c director has a constant direction. For nearly uni-

form textures, we can assume aR and bR to be small compared to unity and keep only the first three terms. Choosing the average c director to lie along the x axis, we can set $\varphi_0=0$. The associated variational energy is then

$$F\approx\tfrac{1}{2}\pi R^2(K_6+K)(a^2+b^2)+2\pi\gamma R+\tfrac{1}{2}\Gamma_1 bR^2\ , \qquad (3.11)$$

where for simplicity we set the Frank constants equal to K. The only variational minimum of Eq. (3.11) is at $a=0$ and $b=-(1/2\pi)\Gamma_1/(K_6+K)$ with the curves of constant c director reducing to lines parallel to the x axis. The resulting texture is a virtual boojum whose core is on the x axis far outside the droplet, so virtual boojum textures should be generally expected for weak boundary conditions. Note that the droplet texture can never be truly uniform, no matter how small Γ_1, which again can be traced to the head-tail asymmetry. The free energy of the nearly uniform texture is

$$F\approx 2\pi\gamma R-\frac{\Gamma_1^2R^2}{8\pi(K_6+K)}\ . \qquad (3.12)$$

The condition $bR\ll 1$ for Eq. (3.10) to apply translates to $R|\Gamma_1|/(K_6+K)\ll 1$. This condition is apparently obeyed for the fatty acid surfactants, but not for the esters. If the droplet retains a circular shape, despite the torque exerted by the mismatch at the boundary, then Γ_1 must be less than the surface energy γ, in which case the second term of Eq. (3.12) is only a small correction.

IV. LINE DEFECTS: LIGHT AND HEAVY WALLS

As mentioned in the Introduction, the hexatic stiffness K_6 of the LC phases studied experimentally so far appears to be rather large compared to the splay and bend Frank constants. The energy of the $m=1$ disclination discussed in Sec. II increases linearly with K_6 [see Eq. (3.6)]. The energy cost might be reduced if the hexatic degree of freedom were uniform across the droplet, thus restricting the texture to the c-director field. This implies that we must relax the condition that the relative angle $\theta-\varphi$ between the c director and the hexatic axes is fixed at one of its equilibrium values. Since such deviations will be energetically costly, we must expect them to be restricted to thin lines stretching across the texture. Line defects are ubiquitous in the observed textures and they are the subject of this section.

The internal structure of line defects must be a transition over a short distance between different equivalent minima of the lock-in potential $V[6(\theta-\varphi)]$. The calculation of the internal structure, by a minimization of Eq. (2.2), is conventional and we will only summarize the results. In the following, the hexatic angle will always be kept fixed at $\theta=0$. A typical line defect in the I and F phases (where V has six minima) will correspond to a rapid change of φ by $\pm 60°$ (a $\pi/3$ line defect). In the L phase, where there are 12 minima, there are two possibilities: (i) a "type-I" chiral wall, where the angle φ changes by 2α and the L phase switches from left- to right-handed chirality (or vice versa); and (ii) a "type-II" chiral wall, where φ changes by $\pi/3-2\alpha$. We can construct an ordinary $\pi/3$ line defect by letting a type-I wall be followed by a type-II wall.

The characteristic width of a line defect as well as its line tension depend on the defect type. For a $\pi/3$ line defect, the tilt field φ must cross a barrier that is essentially controlled by the first Fourier coefficient h_6 of the lock-in potential [see Eqs. (2.2) and (2.3)]. The characteristic widths of a $\pi/3$ line defect are the healing lengths $\xi_6=\sqrt{K_1/h_6}$ for a line defect dominated by splay and $\tilde{\xi}_6=\sqrt{K_3/h_6}$ for a line defect dominated by bend. Splay and bend walls are illustrated in Fig. 7. On dimensional grounds, we must expect that the line tension ε of a $\pi/3$ wall is of order

$$\varepsilon_s\propto h_6\xi_6 \ \text{(splay wall)}\ , \qquad (4.1a)$$

$$\varepsilon_b\propto h_6\tilde{\xi}_6 \ \text{(bend wall)}\ . \qquad (4.1b)$$

In the L phase, both type-I and -II chiral defects are controlled by the second Fourier coefficient h_{12}, except close to the I-L and L-F phase boundaries. Inside the L phase, away from the phase boundaries, the characteristic length scales are $\xi_{12}=\sqrt{K_1/h_{12}}$ for splay walls and $\tilde{\xi}_{12}=\sqrt{K_3/h_{12}}$ for bend walls. The line tensions in this case are found by replacing h_6 by h_{12} in Eqs. (4.1). For $h_6>0$, the rotation 2α of the c director across a type-I wall is smaller than the rotation $\pi/3-2\alpha$ across a type-II wall and consequently the type-I wall has the lower line tension while for $h_6<0$, the situation is reversed. In the Appendix we give an explicit solution of the internal structure of a defect line for a special case.

If a defect line connecting two points A and B were characterized simply by a line tension, then its lowest-energy state would always be a straight line. However, the defect line exists in an anisotropic, hexatic environment. As the line traces its path across a droplet, the angle between the tangent vector of the curve and the hex-

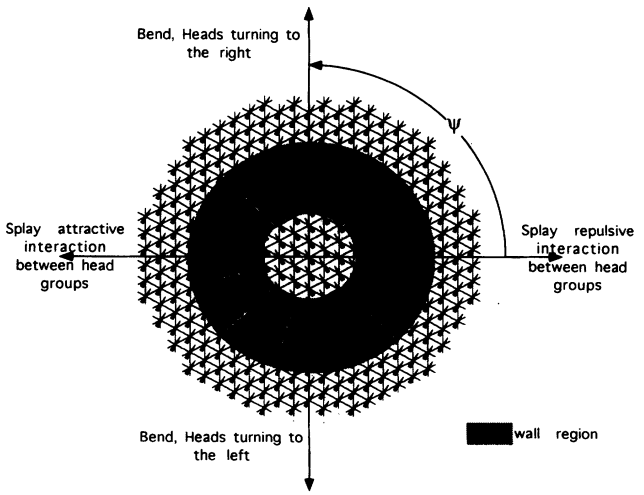

FIG. 7. Two equivalent domains in the F phase, differing by $2\pi/6$ in their tilt azimuth, are separated by domain walls of different orientation. The figure illustrates how the nature of the domain wall (splay or bend) depends on the orientation angle ψ.

atic crystallographic axes varies and the lowest-energy configuration of the defect line need no longer be a straight line. Consider two neighboring domains (1 and 2) of F phase with respective c directors $\hat{\mathbf{c}}_1$ and $\hat{\mathbf{c}}_2$ separated by a $\pi/3$ wall. Let $\bar{\mathbf{c}}=\frac{1}{2}(\hat{\mathbf{c}}_1+\hat{\mathbf{c}}_2)$ and let ψ be the angle between $\bar{\mathbf{c}}$ and the tangent vector of the wall. In Fig. 7 we show the case where domain 2 is a circular region inside domain 1. It shows that when $\psi=0$ and π the wall is pure splay while for $\psi=\pm\pi/2$ the wall is pure bend with hybrid variants at arbitrary angles. Let $\varepsilon(\psi)$ be the angle-dependent line tension. Note from Fig. 7 that the function $\varepsilon(\psi)$ is *not* invariant under a 60° rotation of ψ as would be naively expected. A rotation by $\pm\pi/2$ turns a splay wall into a bend wall and vice versa so we must expect $\varepsilon(\psi)-\varepsilon(\psi+\pi/2)$ to be proportional to K_1-K_3 because this combination controls the difference in energy between splay and bend textures. Examination of Fig. 7 also reveals that $\varepsilon(\psi)$ appears to have a symmetry for a rotation over π. Under this operation, the field lines of the line texture are invariant while their direction is inverted. The head-tail asymmetry of surfactant monolayers breaks the invariance of a texture under inversion of the field lines so $\varepsilon(\psi)-\varepsilon(\psi+\pi)$ must be proportional to some combination of the λ parameters in the free energy, Eq. (2.2).

Since the line tension clearly must be periodic with period 2π, we can always develop $\varepsilon(\psi)$ in a Fourier series:

$$\varepsilon(\psi)=\sum_{n=0}^{\infty} A_n\cos(n\psi) \ . \tag{4.2}$$

The various Fourier coefficients represent the different physical effects discussed above. The A_0 term is the isotropic contribution to the line tension. It is equal to the average $\varepsilon_0\equiv(\varepsilon_s+\varepsilon_b)/2$ of the splay and bend line tensions [see Eq. (4.1)]. The A_1 term must be proportional to a combination of the λ parameters and the A_2 term must be proportional to K_1-K_3. An explicit calculation shows (see the Appendix) that

$$A_1=\pm\left[\frac{\lambda_b+\lambda_s}{5}+\frac{\lambda_b-\lambda_s}{7}\right] \quad (I,F \text{ phase}) \ , \tag{4.3a}$$

$$A_2=\varepsilon_0\left[\frac{K_1-K_3}{K_1+K_3}\right] \ . \tag{4.3b}$$

The value of A_1 in the L phase is more complex and is discussed in the Appendix. It follows from Eqs. (2.8), (2.9), (4.1), and (4.3) that A_1/A_0 and A_1/A_2 are both of the order of ζ/ξ, the ratio of the two characteristic length scales of our problem discussed in Sec. II. For the textures studied so far this ratio is small, so the contribution of the $n=1$ term to the Fourier series is expected to be *smaller* than that of the $n=2$ term. Indeed, let A and B be the initial and final points of the defect lines and s the arc length along the defect line with, as before, $\psi(s)$ the local angle between the tangent vector to the defect line and $\bar{\mathbf{c}}$. Keeping the end points fixed, the contribution to the total line energy ΔE from the $n=1$ term in Eq. (4.2) is proportional to

$$\Delta E_1 \propto \int_A^B \cos[\psi(s)]ds \propto \hat{\mathbf{y}}\cdot\int_A^B \hat{\mathbf{t}}(s)ds \propto \hat{\mathbf{y}}\cdot\mathbf{R}_{AB} \tag{4.4}$$

with $\hat{\mathbf{t}}(s)$ a unit vector tangent to the defect line and $\hat{\mathbf{R}}_{AB}$ the distance between A and B. This energy is, according to Eq. (4.4), not dependent on the path taken by the defect line, so in determining the optimal path of the defect line between fixed points, we can neglect the first term of the Fourier series. The $n=2$ term in Eq. (4.2) is thus the lowest-order term, which is sensitive to the path of the defect line (apart from the isotropic line tension).

Assume first that $K_1<K_3$. The $n=2$ term is then minimized by choosing $\psi=0$ or π, i.e., a splay wall. Consider such a splay wall with a tangent along the y axis so the c directors $\hat{\mathbf{c}}_1$ and $\hat{\mathbf{c}}_2$ of the two adjacent domains make angles of $\pm 30°$ with the y axis. On the other hand, a bend wall lying along the x axis, with $\psi=\pm\pi/2$ and $\hat{\mathbf{c}}_1$ and $\hat{\mathbf{c}}_2$ making angles of $\pi/2\pm 30°$ with the x axis, would maximize the $n=2$ term. We thus can call a splay wall "light" and a bend wall "heavy." Now assume that we begin with a splay wall and increase K_1 (say, by changing the temperature) until it exceeds K_3. The bend and splay walls exchange their roles as light and heavy walls. If, however, we keep the initial and final points A and B of the defect line fixed at their original positions (at, for instance, the center and one of the vertices of a hexagonal droplet) and also keep the two domain orientations $\hat{\mathbf{c}}_1$ and $\hat{\mathbf{c}}_2$ fixed, then the wall is, in a sense, frustrated. The splay wall would like to turn into a bend wall to lower the line tension, but it can do so only by letting the direction of the wall point away from the y axis. This would indeed lower the local line tension, but it also increases the overall length of the line, thereby raising the contribution of the isotropic $n=0$ term to the line energy. The true configuration of the defect line must result from some compromise between these two effects.

As an example, a straight wall along the y axis, with $\psi=0$, has, using Eqs. (4.2) and (4.3), a line energy of

$$\Delta E_{\text{straight}}\approx 2L\varepsilon_0\left[\frac{K_1}{K_1+K_3}\right] \tag{4.5a}$$

with L the distance between the end points A and B. Alternatively, we could choose a defect path with a 90° kink in the middle with $\psi=\pm\pi/4$ along the two legs of the kink. This would have an energy

$$\Delta E_{\text{kink}}\approx 2\sqrt{2}L\varepsilon_0 \ . \tag{4.5b}$$

If $K_1/K_3>1/(\sqrt{2}-1)$, then the kink solution has a lower energy, while in the opposite case we must choose the straight-line configuration. The threshold for the appearance of kinks with arbitrary kink angle is $K_1/K_3=2$. The kink angle δ_K starts from 180° and gradually decreases as we increase K_1 (Fig. 8):

$$\delta_K=\pi-2\arccos\left[\frac{1}{K_1/K_3-1}\right]^{1/2} \ . \tag{4.6}$$

We thus must expect a progressive reorganization of the texture of the droplets characterized by the appearance of kinks as we cross the threshold $K_1/K_3=2$ from below. If we had started with a straight bend wall for $K_1>K_3$, kinks would have appeared at a critical value *less* than K_3 as we reduced K_1. In other words, the changes in the

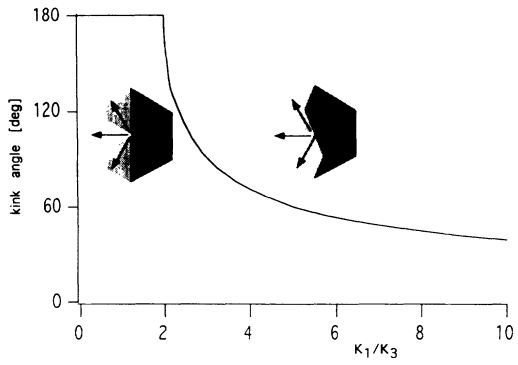

FIG. 8. Dependence of the kink angle δ_K on the ratio K_1/K_3 for a droplet with strong perpendicular boundary conditions to the isotropic phase. Starting at $K_1/K_3=2$, kinks smoothly evolve by decreasing the kink angle from π to lower values.

texture around $K_1=K_3$ should be characterized by a noticeable hysteresis.

V. DROPLET TEXTURES

A. Basic motif revisited

We now will return to the general problem of droplet textures, using the results obtained in Secs. III and IV to construct a catalog of stable droplet textures as allowed by our continuum free energy. In the Introduction we discussed the basic motif of most observed droplet textures: a central radial defect with six line defects emerging from the core [Figs. 4(a)–4(c)]. The drop is either circular, hexagonal, or rosette shaped. In each of the six segments, the director is roughly uniform and normal to the boundary. We will want to compare the energy cost associated with the variations on the basic motif. In order to do so, we must start with an estimate of the energy cost of the texture of the basic motif itself.

We first will assume a perfectly hexagonal drop. In the language of Sec. IV, the six segments of the drop are bordered by six $\pi/3$ splay walls where the director makes a 60° rotation (either $\psi=0$ or $\psi=\pi$ splay walls). The free energy of the basic motif with a purely hexagonal shape is then

$$F=6R_H\varepsilon_0\left\{\frac{2K_1}{K_1+K_3}\right\}+6R_H\{\gamma-|\bar{\Gamma}_1|-\Gamma_2\}+E_c(b) \tag{5.1}$$

with R_H the radius of a circle circumscribing the hexagon. The first term in Eq. (5.1) is the energy of the six line defects obtained from Eq. (4.5a). The second term is the usual LE-LC interfacial energy, while the third term is the core energy of the central defect. The core of the central defect and its energy $E_c(b)$ may differ from that of the $m=1$ disclination of Sec. III [22].

The energy calculated from Eq. (5.1) may be compared with $6\gamma R_H$, the energy of a droplet with a nearly homogeneous texture [see Eq. (3.12)]. The condition for the basic motif to have a lower energy than a uniform hexagonal drop is

$$R_H>\frac{\frac{1}{6}E_c(b)}{\{|\bar{\Gamma}_1|+\Gamma_2\}-\varepsilon_0\left\{\frac{2K_1}{K_1+K_3}\right\}}\,. \tag{5.2}$$

We conclude that if the anisotropic contribution to the interfacial energy exceeds the defect line tension

$$|\bar{\Gamma}_1|+\Gamma_2>\varepsilon_0\left\{\frac{2K_1}{K_1+K_3}\right\}, \tag{5.3}$$

then there is a critical radius

$$R_c=\frac{\frac{1}{6}E_c(b)}{\{|\bar{\Gamma}_1|+\Gamma_2\}-\varepsilon_0\left\{\frac{2K_i}{K_1+K_3}\right\}} \tag{5.4}$$

beyond which coexistence droplets *must* have a texture in their ground-state configuration (although of course not necessarily the basic motif). Recall that we reached similar conclusions in the discussion of the $m=1$ disclination. Notice that the critical radius is not one of our "natural" length scales. It is controlled by the core energy of the central defect in the basic motif. Droplets with radii smaller than R_c have (nearly) uniform textures. If the inequality Eq. (5.3) is not obeyed, then the (nearly) uniform texture has a lower energy than the basic motif for any droplet radius. In the present model we thus must assume that the fatty acids, which have nearly uniform droplet textures, violate Eq. (5.3) while the esters, which exhibit the basic motif or one of its variations, obey it.

We can also compare the basic motif with the $m=1$ splay disclination in a circular drop discussed in Sec. III. The basic motif has a lower energy provided

$$(K_6/K_1)>\left\{C_1\left[\frac{K_1}{K_1+K_3}\right](R/\zeta_6)+C_2\left[\frac{E_c(b)-E_c(m=1)}{K_1}\right]+C_3R\left[\frac{\gamma-|\bar{\Gamma}_1|}{K_1}\right]\right\}\Big/\ln(R/a_0)\,, \tag{5.5}$$

with the C_i's positive numbers of order one. The second term is due to the difference in core energies of the two textures, while the last term is due to the fact that the perimeter of a hexagon (or rounded hexagon) exceeds that of a circle of the same area as the hexagon. If we assume that both the core energies and the Frank constants are of order k_BT, then the first and third terms dominate for droplet radii of order 100 μm (assuming ζ_6 to be a few micrometers and γ, which must exceed $|\Gamma_1|$, to be of order k_BT/a_0).

As we argued in the Introduction, the observed stability of the basic motif requires the hexatic rigidity to exceed the Frank constants. The surprise is how large the hexatic rigidity actually must be for the basic motif to be stable. According to Eq. (5.5), for large enough droplet radii R the basic motif always has a higher energy than the $m=1$ disclination. The reason is that the energy of an $m=1$ disclination increases only logarithmically

with R while the energy of the basic motif increases linearly. For droplets of radius 100 μm, the first term of Eq. (5.5) requires K_6 to be more than an order of magnitude larger than K_1. The third term would increase this estimate even more. The absence of certain textures thus gives us important information about the various constants entering in the free energy.

B. Droplet shape

The geometrical signature of a coexistence drop that can be probed most easily is its shape. The basic motif is a perfect hexagon, but real coexistence drops are not perfect hexagons. Their shape normally ranges from circular to rounded hexagons. It could be thought that this is simply due to the effect of thermal fluctuations, which always tend to round two-dimensional facetted structures because of thermal roughening [18]. However, more recently six-petalled rosette-shaped droplets have also been seen which would be difficult to explain as a roughening effect and we will ignore thermal fluctuations in the following. The shape of a droplet is in general determined by the various contributions to Eq. (5.1): the LE-LC line tension γ, the strength Γ_1 of the normal boundary conditions, and finally the line energy ε_0 of the $\pi/3$ defect lines. One would expect three types of shapes for a fixed given droplet area: a circular shape (with a weak sixfold modulation) for $\gamma \gg |\Gamma_1|$, a hexagonal shape for $|\Gamma_1|$ of order γ, and finally a rosette shape for large ε_0. A circular shape obviously has the lowest energy when the isotropic LE-LC line tension is large, while large $|\Gamma_1|$ imposes normal boundary conditions on the c director, and thus a hexagonal shape, at the price of an increased interfacial perimeter.

To see how a rosette shape can occur, set $\Gamma_1=0$ and let β be the angle of contact between the defect line and the LE-LC boundary. If $\varepsilon_0=0$, then this angle is 90°, while for finite ε_0 Young's law must be obeyed at the intersection point where the defect line meets the LE-LC phase boundary:

$$\varepsilon_0 \frac{2K_1}{K_1+K_3} = 2\gamma \cos\beta \ . \tag{5.6}$$

As we increase ε_0 with respect to γ, β falls below 90° and the circle transforms into a six-sectored rosette whose perimeter consists of segments of circles. The reason that the boundary must consist of circle segments is that the pressure inside the coexistence drop is uniform (as it is a liquid). For $\Gamma_1=0$ Laplace's law must be obeyed, which requires that the pressure drop across the interface equals the product of the interface curvature and the interface tension. Since the interface curvature is a constant, the boundary must be a circle segment. Note that we must demand that the line tension is not too great

$$\varepsilon_0 \frac{2K_1}{K_1+K_3} < 2\gamma \tag{5.7}$$

for the rosette to be stable.

We cannot directly use Young's law for finite Γ_1 because the anisotropy of the boundary condition implies that a torque is exerted at the intersection point. However, for a sixfold symmetric droplet texture with six defect lines connecting the center of the drop to six intersection points at the LE-LC boundary, and with uniform texture inside the six sectors of the drop, the Γ_1 term in Eq. (2.5) can be written as

$$\begin{aligned} F_l &\approx \oint [\gamma - \Gamma_1 \hat{\mathbf{c}}(s)\cdot\hat{\mathbf{n}}(s) + \cdots]ds \\ &\approx \oint (\gamma - \Gamma_1 \hat{\mathbf{c}}\cdot\hat{\mathbf{z}}\times\hat{\mathbf{t}}(s) + \cdots)ds \\ &\approx \sum_{\text{sectors}} (\gamma P_s - |\Gamma_1| C_s) \ . \end{aligned} \tag{5.8}$$

Here $\hat{\mathbf{t}}(s)$ is a unit vector tangent to the LE-LC interface, P_s is the perimeter of a sector, and C_s is the length of a chord inside a segment stretching between two of the intersection points. The Γ_1 term thus behaves like a (negative) line tension acting on the line segments connecting the intersection points and tends to increase the chord lengths. We can still use Young's law, provided we include the negative line tensions of the six chords. The result is

$$\varepsilon_0 \frac{2K_1}{K_1+K_3} - |\Gamma_1| = 2\gamma \cos\beta \ . \tag{5.9}$$

If $|\Gamma_1|$ is less than $\varepsilon_0 2K_1/(K_1+K_3)$, we retain the rosette shape. In the opposite case, β must exceed 90°, which means that the droplet has a hexagonal shape. A perfect hexagon would correspond to $\beta=120°$, which is reached when $|\Gamma_1|$ equals $\varepsilon_0[2K_1/(K_1+K_3)]+\gamma$. But as we saw earlier, $|\Gamma_1|$ cannot exceed γ for reasons of thermodynamic stability, so we conclude that droplets with the basic motif are at best hexagons with rounded edges.

In summary, for γ large compared to both ε_0 and Γ_1, the shape is roughly circular; for ε_0 comparable to γ and both large compared to Γ_1, the shape is a rosette with apex angle β given by Eq. (5.6); and for Γ_1 and γ comparable and both large compared to ε_0, the shape is a rounded hexagon, with the transition from rounded hexagon to rosette taking place at $\varepsilon_0[2K_1/(K_1+K_3)]=|\Gamma_1|$.

C. Dodecagonal droplets

For L-phase droplets, the $\pi/3$ wall can break up into a type-I and a type-II wall, as we saw in Sec. III. One of these two walls will then be "high contrast" and one "low contrast" in terms of fluorescence and Brewster-angle studies (since the contrast should increase with the magnitude of the rotation of the director across a wall). Type-I and type-II walls can either repel or attract (depending on the relative magnitudes of K_1-K_3 and the head-tail asymmetry). The sign of the interaction and the energy cost of the intersection points between defect lines and the phase boundary determine the minimum energy configuration, which is either type-I walls halfway between type-II walls or type-I walls bound to type-II walls. The first possibility would produce a dodecagonal-shaped droplet with 12 defect lines of alternating high and low contrast [Fig. 4(f)]. The shape should not be a perfect dodecagon; however, because a low contrast defect line is

not expected to deform the droplet shape as much as a high contrast defect line.

D. Chiral textures

In the discussion of locked droplet textures in Sec. II, we saw that the appearance of spiral textures was associated with the onset of chiral symmetry breaking in the L phase, with the pitch of the spiral proportional to the chiral order parameter. In this section we will explore what happens to the basic motif when the L phase is entered. The 12-fold structure of Fig. 4(f) is associated with alternating left and right chiral domains, which try to curve in opposite directions, thereby producing no net chirality in the droplet. We thus will focus on the other configuration [Fig. 4(d)], where type-I and type-II walls are bound together, leaving only domains of one kind of chirality. The question is whether we now can use the net chiral deformation of the six defect lines of the basic motif as a measure of the chiral order parameter of the L phase, since such deformations are directly observable in optical studies.

To investigate the stability of the basic motif against chiral deformation, assume we have a (nearly) hexagonal droplet and that the defect line tension is small compared to the interfacial energy. Now consider one of the six segments of the basic motif and choose the x axis to lie along the director. The two line defects that form the boundary of the segment emerge from the origin and make angles of $\pm\pi/6$ with the x axis. We will assume that the c director and the hexatic axis remain locked together in the interior of the segment. To investigate the stability we allow small excursions of the director away from the x axis. For $K_1 \approx K_3$, the rotation angle φ of the c director with respect to the x axis produced by the perturbation must obey Laplace's equation [$\Delta\varphi=0$; see Eq. (3.3)]. If we demand that this angle is zero at the LE-LC boundary, we must impose as boundary condition $\varphi[x=R(\sqrt{3}/2),y]=0$ on the solution of Laplace's equation. The appropriate solution of Laplace's equation corresponding to a bend texture associated with the onset of chirality is

$$\varphi(x,y)=k\left[x-\frac{R}{2}\sqrt{3}\right], \tag{5.10}$$

with k an undetermined constant, which can be identified as the "vorticity" $\hat{\mathbf{z}}\cdot\nabla\times\hat{\mathbf{c}}$ of the texture. Here $kR \ll 1$ because we are only testing the stability of the basic motif, so we will expand the free energy of the wedge in powers of kR. The textural energy cost per unit area is proportional to K_6k^2 while the energy gain is proportional to $\lambda_b k$, which always produces a nonzero vorticity upon minimization. A straightforward calculation shows that allowing curvature in the texture lowers the free energy by

$$\Delta F=-\frac{1}{2}A\frac{\lambda_b^2\sin^2 6(\theta-\phi)_{\rm eq}}{(K_6+K_3)} \tag{5.11a}$$

with A the droplet area. The vorticity

$$k=\lambda_b\frac{\sin 6(\theta-\phi)_{\rm eq}}{K_6+K_3} \tag{5.11b}$$

is proportional to the chiral order parameter X.

We now consider the effect of the curvature of the texture on the defect line. The defect-line energy was discussed in Sec. IV:

$$E=\int ds\,\varepsilon_0\left[1-\frac{K_3-K_1}{K_3+K_1}\cos[2\psi(s)]\right] \tag{5.12}$$

with, as before, ψ the angle between the tangent to the defect line and the average c director on opposite sides of the line. The line integral is along one of the defect lines whose initial and final points are kept fixed, so we do not include the shape-independent first-order term in the Fourier series. Because of the curvature of the texture inside the wedge, the angle ψ is forced to deviate away from its optimal value of zero or π. The restoring torque will tend to reduce the vorticity of the texture inside the wedge, but it is easy to show that for $kR \ll K_6/\varepsilon$ we may neglect this effect.

Assuming k thus to be given by Eq. (5.11b), we minimize Eq. (5.12) by allowing the defect line to be deformed away from a straight line. Let $y(s)$ be the displacement of the defect line along the normal of the undeformed line. For small $y(s)$, this gives

$$E=\varepsilon_0\int_0^R ds\left[\frac{1}{2}\frac{2K_1}{K_1+K_3}y'(s)^2+2\frac{K_3-K_1}{K_3+K_1}\left[y'(s)-\frac{\sqrt{3}}{2}k(R-s)\right]^2\right]. \tag{5.13}$$

The first term is the usual defect line tension while the second term is the restoring energy, which tries to reduce ψ to zero. Minimizing Eq. (5.13) gives the optimal shape of the defect line, which is found to be a parabola with curvature:

$$y''=k\frac{\sqrt{3}(K_3-K_1)}{2K_3+K_1}. \tag{5.14}$$

The curvature of the defect line is thus of order k, the vorticity of the bend texture inside the segment. The full structure of the perturbed droplet is shown in Fig. 3(d). The line defect curvature y'' is experimentally directly accessible. Since the vorticity is, according to Eq. (5.12b), proportional to the chiral order parameter, the appearance of a spiral shape in the defect lines is indeed a signature of the L phase.

There is, however, a caveat to this prediction. We saw that for infinite samples, the ground state of the texture can be a periodic array of $\pi/3$ splay walls due to the head-tail asymmetry, an effect which is *not* a signature of the L phase. The characteristic stripe spacing is of the order of the length ξ. If we start with a coexistence drop with a basic motif and allow the drop to grow in size, it could nucleate a sixfold Archimedean spiral (i.e., a spiral with a fixed spacing between adjacent arms) [23]. The

spacing would be of the order of the equilibrium width of a splay wall, so that far from the defect core the texture would locally assume its ground-state structure. For large but finite droplet radii, with R comparable to or larger than ξ, one could expect spiral structures completely unrelated to the chiral phase. This would, however, demand a nonuniform splay-type texture inside the six segments rather than a bend texture discussed in this section, which could not be consistent with the normal boundary conditions at the LE-LC phase. Whether embryonic Archimedean spirals really can be ruled out would have to be determined experimentally by a careful quantitative study of the texture inside the segments.

E. Kinked droplet textures

Finally, we consider the competition between splay and bend inside a droplet. We saw in Sec. IV that a $\pi/3$ splay defect line prefers to be straight if $K_1 < 2K_3$, while for $K_1 > 2K_3$, it prefers to have a kink (Fig. 8) whose angle decreases from π as K_1 increases (when a bend wall is the light defect). In the context of a coexistence droplet, this means that along the LE-LC coexistence line there can be a critical temperature and pressure, where $K_1 = 2K_3$, which should mark the reorganization of the texture of the droplet. Once K_1 exceeds $2K_3$, the six defect lines prefer be kinked [Fig. 4(e)]. If we assume strictly uniform textures in the interior of the six segments, then each defect line could have a kink displacement that is arbitrarily to either side of the defect line, as long as the kink angle is so small that there is no steric interaction between the six walls. However, since for $K_1 > 2K_3$ a kinked defect line is not a pure bend wall—the stable configuration—it must deform the texture inside the segments. In addition, because of the surface-ferroelectric terms, the texture inside the segments is in general not quite uniform. For these reasons, the texture is expected to mediate an interaction between the kinks on different defect lines. Although the problem is computationally involved, this interaction is likely to be repulsive. This means, at least in the L phase, that the kinks will all tend to deform in the same direction, producing a kinked spiral [Fig. 4(d)]. The appearance of a kinked spiral inside a droplet thus should not be used as an indicator of chiral symmetry breaking.

VI. CONCLUSIONS

We have shown that the phenomenological free energy Eq. (2.2) leads to a variety of domain structures for droplets of hexatic monolayer phases surrounded by an isotropic phase. Experiments on Langmuir and Gibbs monolayers are generally in accord with the picture outlined in this paper; nearly every kind of texture discussed in the paper has been observed in experiments. Indeed, one of the textures, the rosette, was observed experimentally [12] only after it had emerged from the theory. To our knowledge the dodecagonal structure that we predict for the L phase has not yet been observed, but it is not clear if the tilt-angle resolution of the experimental techniques is sufficiently high to show the presence of both types of defect lines. (A closely related structure has been seen, however, in films of tilted hexatic liquid crystals [24].)

The polarized fluorescence and Brewster-angle microscope images show spatial variations in the tilt azimuth but do not immediately provide values of azimuth itself. In principle, the tilt azimuth can be determined from the fluorescence studies, but this requires a knowledge of both the orientation of the transition moment of the probe with respect to the axis of the surfactant molecule and the tilt angle. Nevertheless, it is possible to determine some information about the tilt azimuth from the symmetry of the images and the variation in contrast with the direction of the incident radiation [10] and one finds qualitative agreement with the theory.

The relation between the Brewster-angle images and the tilt azimuth is more direct because the contrast arises from a property of the surfactant itself rather than from a probe. A full analysis of the tilt structure of a domain requires a careful study of the variation in intensity as a function of the polarization; this has not yet been done for monolayers at the air-water interface. Overbeck, Hönig, and Möbius [13] have used the method of Berreman [25] to calculate the textures that would be observed for a variety of domain structures consistent with those described here and find that the calculated patterns closely resemble those that have been observed.

Not all of the experiments are consistent with the theory however. In recent work, Rivière, Hénon, and Meunier [19] examined striped textures in Gibbs monolayers of sodium myristate by Brewster-angle microscopy and determined that the variation in the tilt azimuth across each stripe was $95° \pm 10°$. On the other hand, fluorescence studies of stripes in Langmuir monolayers of pentadecanoic acid seem to be consistent with a 60° variation in the tilt azimuth, but no quantitative comparison with the theory could be carried out [26]. It is possible that for sodium myristate the hexatic stiffness K_6 is comparable to the Frank constants K_1 and K_3. Combined rotations of the director and bond-angle fields across a stripe would then produce a variation in the tilt azimuth different from 60°. Coexistence droplets with textures that differ from those that we have predicted are also observed. These include structures (for example, those containing two kinked defect lines) whose symmetry is difficult to reconcile with the hexatic order and the boundary conditions at the droplet interface.

Studies of the variations of textures with the chain length of the amphiphile, which are now underway, will allow a check on the consistency of the theory, but a rigorous test will require a knowledge of a large number of substance-dependent constants. Estimates of some of them can be obtained from observations of the variations of angles between tilt regions [9] and fluctuations in defect lines [19], but experiments similar to those carried out on films of liquid crystals by Rosenblatt *et al.* [27] must be carried out.

Finally, it is implicit in the analysis of the textures that the monolayer phases are hexatics. The structures of the monolayer phases of the fatty acids are now reasonably well known, but no diffraction studies have been carried out as yet on esters. A miscibility study of ester-acid

mixtures [3] has allowed the phases in the esters to be correlated to those of the acids, but there is still a great deal of uncertainty about the nature of the ester phases. In particular, the regions of stability of the L phase remain unknown.

ACKNOWLEDGMENTS

The work was supported by the Donors of the Petroleum Research Fund administered by the American Chemical Society and by the NSF. T. F. acknowledges additional support under the F. Lynen program of the Alexander von Humboldt Foundation. We are grateful to J. Meunier for providing the image of the boojum in Fig. 2. We thank him and S. Hénon, I. Peterson, J. Selinger, and F. Rondelez for helpful discussions.

APPENDIX

In the limit of vanishing head-tail asymmetry and isotropic Frank constants ($K_1=K_3$) the structures of the domain walls may be calculated analytically. Being stationary solutions to the free energy they obey the equation

$$\frac{K_1K_6}{K_1+K_6}\frac{d^2(\theta-\varphi)}{dx^2}=\frac{dV}{d(\theta-\varphi)}\ , \tag{A1}$$

with $(\theta-\varphi)$ having equilibrium values at $x=\pm\infty$ The solutions of this equation are

$$(\theta-\varphi)_I(x)=\frac{1}{3}\text{arccot}\left\{-\sinh\left[6\left[\frac{K_1+K_6}{K_1K_6}h_6\right]^{1/2}x\right]\right\}, \tag{A2a}$$

$$(\theta-\varphi)_F(x)=\frac{\pi}{6}+(\theta-\varphi)_I(x)\ , \tag{A2b}$$

$$(\theta-\varphi)_{L_I}(x)=\frac{1}{3}\arctan\left\{\left[\frac{1+\sigma}{1-\sigma}\right]^{1/2}\tanh\left[\frac{3}{2}\sqrt{1-\sigma^2}\left[-h_{12}\frac{K_1+K_6}{K_1K_6}\right]^{1/2}x\right]\right\}, \tag{A2c}$$

$$(\theta-\varphi)_{L_{II}}(x)=\frac{1}{3}\arctan\left\{-\left[\frac{1+\sigma}{1-\sigma}\right]^{1/2}\coth\left[\frac{3}{2}\sqrt{1-\sigma^2}\left[-h_{12}\frac{K_1+K_6}{K_1K_6}\right]^{1/2}x\right]\right\}, \tag{A2d}$$

with $\sigma=h_6/4h_{12}$.

Solution (A2a) refers to the I phase, (A2b) to the F phase, and (A2c) and (A2d) to the two walls in the L phase. In the I and F phases, h_{12} is unimportant and it has therefore been set to zero. The length scales of Sec. IV are found in the limit $K_6\gg K_1$ in the I and F phase and, additionally, for $\sigma\to 0$ in the L phase (inside the L phase, not at the boundaries).

The orientation dependence of the domain wall energy is found to first order in the Frank constant anisotropy and the head-tail asymmetry by using the solutions (A2), which are degenerate in energy with respect to the angle ψ (see Sec. IV and Fig. 5 for the definition of ψ), as trial states for the total free energy (2.2). We find for the domain wall energy per unit length in the I and F phase:

$$\varepsilon=\varepsilon_{I,F}\left[1+\frac{K_1-K_3}{K_1+K_3}\cos(2\psi)\right] \pm\left[\frac{\lambda_b+\lambda_s}{5}+\frac{\lambda_b-\lambda_s}{7}\right]\cos(\psi)\ , \tag{A3a}$$

where the + sign refers to the I phase and the − sign to the F phase. In the L phase we find

$$\varepsilon=\varepsilon_{L_I}\left[1+\frac{K_1-K_3}{K_1+K_3}\cos(2\psi)\right] -2\left[\frac{\lambda_b+\lambda_s}{5}\sin[5(\theta-\varphi)_{\min}] -\frac{\lambda_b-\lambda_s}{7}\sin[7(\theta-\varphi)_{\min}]\right]\cos(\psi)\ , \tag{A3b}$$

$$\varepsilon=\varepsilon_{L_{II}}\left[1+\frac{K_1-K_3}{K_1+K_3}\cos(2\psi)\right] -2\left[\frac{\lambda_b+\lambda_s}{5}\sin[5(\theta-\varphi)_{\min}-5\pi/6] -\frac{\lambda_b-\lambda_s}{7}\sin[7(\theta-\varphi)_{\min}-7\pi/6]\right]\cos(\psi) \tag{A3c}$$

for the type-I and type-II walls, respectively. The terms A_0, A_1, and A_2 can be easily read off from Eqs. (A3). Note that if the minimum energy is the splay configuration with lower head density in the I phase, then the minimum energy in the F phase is the splay with higher head density. The same is true for the type-I and type-II walls well inside the L phase.

[1] D. R. Nelson and B. I. Halperin, Phys. Rev. Lett. **41**, 121 (1978); Phys. Rev. B **19**, 2457 (1979).
[2] S. B. Dierker, R. Pindak, and R. B. Meyer, Phys. Rev. Lett. **56**, 1819 (1986).
[3] A. M. Bibo, C. M. Knobler, and I. R. Peterson, J. Phys. Chem. **95**, 5591 (1991).
[4] C. G. Lyons and E. K. Rideal, Proc. R. Soc. London Ser. A **124**, 322 (1929); D. G. Dervichian, J. Phys. Chem. **7**, 931 (1939).
[5] For a recent review of monolayer phases, including evidence for the existence of hexatics, see C. M. Knobler and R. C. Desai, Annu. Rev. Phys. Chem. **43**, 207 (1992), and the references therein.
[6] A summary of the different phases in smectic liquid crystals can be found in G. W. Gray and J. W. Goodby, *Smectic Liquid Crystals–Textures and Structures* (Leonard-Hill, Glasgow, 1984).
[7] X. Qiu, J. Ruiz-Garcia, K. J. Stine, C. M. Knobler, and J. Selinger, Phys. Rev. Lett. **67**, 703 (1991).
[8] G. A. Overbeck and D. Möbius, J. Phys. Chem. **97**, 7999 (1993).
[9] S. Hénon and J. Meunier, J. Chem. Phys. **98**, 9148 (1993).
[10] J. Ruiz-Garcia, X. Qiu, M.-W. Tsao, G. Marshall, C. M. Knobler, G. Overbeck, and D. Möbius, J. Phys. Chem. **97**, 6955 (1993).
[11] P. G. de Gennes, *The Physics of Liquid Crystals* (Clarendon, Cambridge, 1974).
[12] B. Fischer, M.-W. Tsao, and C. M. Knobler (unpublished).
[13] G. A. Overbeck, D. Hönig, and D. Möbius, Thin Solid Films **242**, 213 (1994).
[14] D. R. Nelson and B. I. Halperin, Phys. Rev. B **21**, 5312 (1980).
[15] J. V. Selinger and D. R. Nelson, Phys. Rev. Lett. **61**, 416 (1988); Phys. Rev. A **39**, 3135 (1989).
[16] J. V. Selinger, in *Complex Fluids*, edited by E. B. Sirota, D. Weitz, T. Witten, and J. Israelachvili, MRS Symposia Proceedings No. 248 (Materials Research Society, Pittsburgh, 1992), p. 29; J. V. Selinger, Z.-G. Wang, R. F. Bruinsma, and C. M. Knobler, Phys. Rev. Lett. **70**, 1139 (1993).
[17] R. B. Meyer and P. S. Pershan, Solid State Commun. **13**, 989 (1973).
[18] See, for example, *Statistical Mechanics of Membranes and Surfaces*, edited by D. Nelson, T. Piran, and S. Weinberg (World Scientific, Singapore, 1989).
[19] S. Rivière S. Hénon, and J. Meunier, Phys. Rev. E **49**, 1375 (1994).
[20] S. A. Langer and J. P. Sethna, Phys. Rev. A **34**, 5035 (1986).
[21] G. A. Hinshaw, Jr. and R. G. Petschek, Phys. Rev. A **39**, 5914 (1989).
[22] There are now two distinct regions inside the core. At a radius of order ζ, it becomes impossible for the director to remain uniform in each of the six segments, and the texture transforms to that of an $m=1$ point disclination, except that the hexatic degree of freedom does not participate. Then, within a radius of order of the microscopic length scale a_0, the continuum theory must again break down.
[23] J. V. Selinger (private communication).
[24] J. Maclennan and M. Seul, Phys. Rev. Lett. **69**, 2082 (1992).
[25] D. W. Berreman, J. Opt. Soc. Am. **62**, 502 (1972).
[26] D. K. Schwartz, J. Ruiz-Garcia, X. Qiu, and C. M. Knobler, Physica A **204**, 606 (1994).
[27] C. Rosenblatt, R. Pindak, N. A. Clark, and R. B. Meyer, Phys. Rev. Lett. **42**, 1220 (1979).

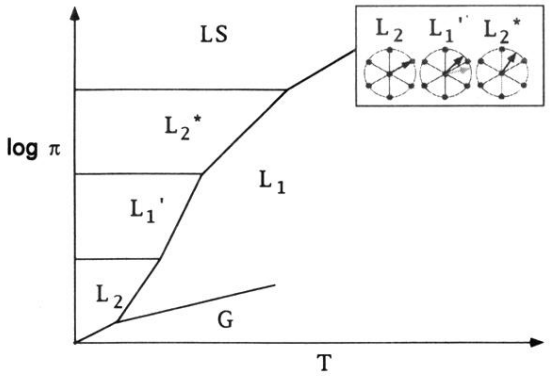

FIG. 1. Schematic pressure-temperature (π-T) phase diagram showing several of the monolayer phases that have been identified in fatty acids and their esters. The relative locations of the gas (G), liquid-expanded (L_1), and superliquid phases (LS) are much the same for many substances. The locations of the other phases and the positions of the boundaries between them are more variable and less well known. The inset shows the orientation of the molecular tilt azimuth with respect to the local sixfold structure of the head groups that exists in the three tilted hexatic phase L_1', L_2, and L_2^*.

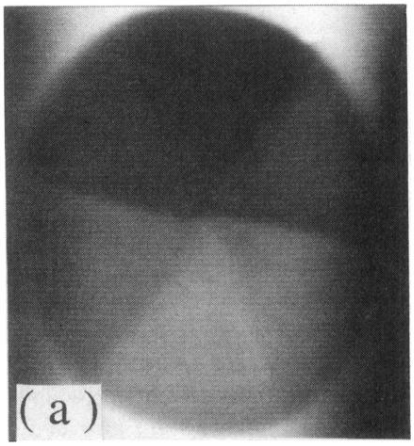

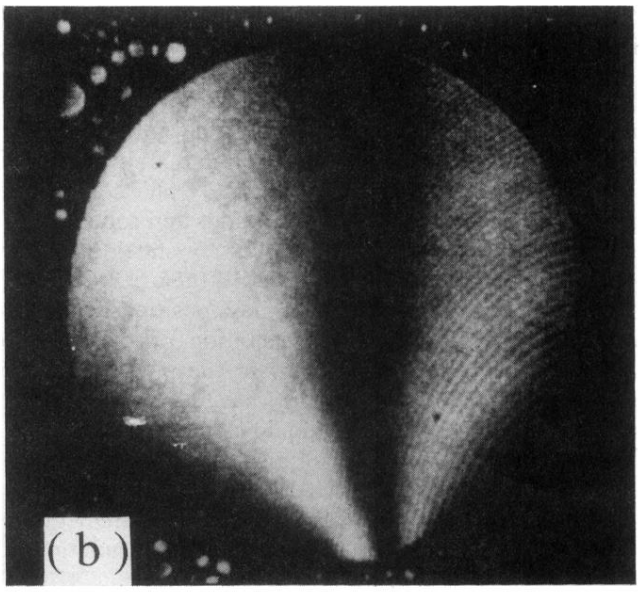

FIG. 2. Images of droplet textures. The droplets are surrounded by the liquid expanded phase, which is isotropic. (a) Polarized fluorescence microscope image of a star defect in a monolayer of methyl octadecanoate. (b) Brewster-angle microscope image of a boojum in a monolayer of pentdecanoic acid (courtesy J. Meunier).

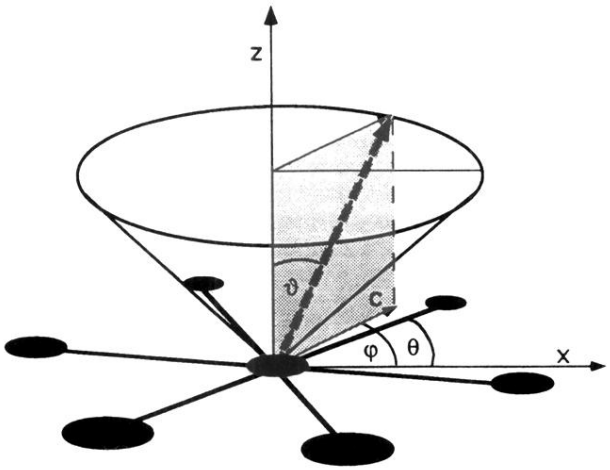

FIG. 3. Definition of the bond angle θ, the tilt angle ϑ, the tilt azimuth φ, and the director c.

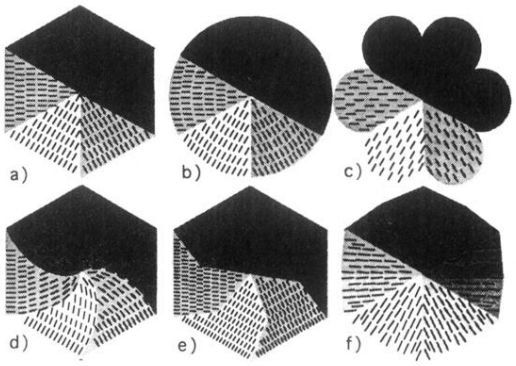

FIG. 4. Droplet textures for hexatic phases. The lines indicate the orientation of the molecular tilt azimuth within each domain and the shading gives an impression of the contrast that would be observed in an image obtained by polarized fluorescence microscopy.

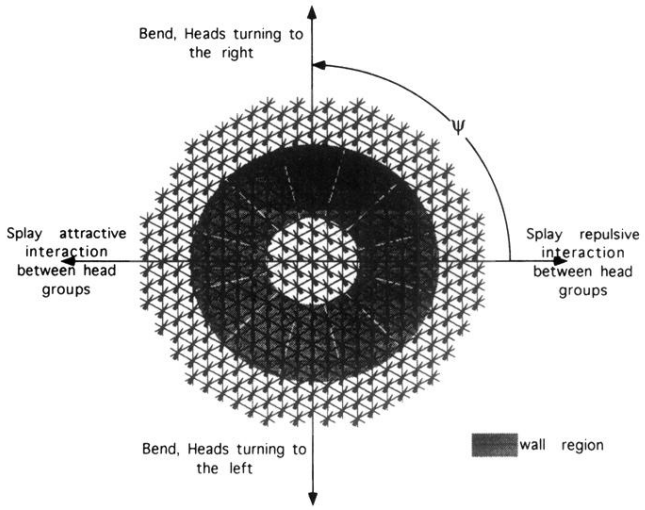

FIG. 7. Two equivalent domains in the F phase, differing by $2\pi/6$ in their tilt azimuth, are separated by domain walls of different orientation. The figure illustrates how the nature of the domain wall (splay or bend) depends on the orientation angle ψ.

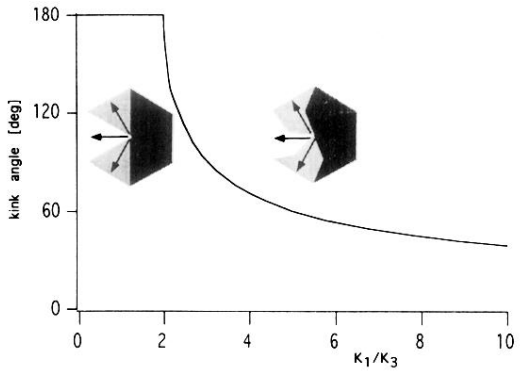

FIG. 8. Dependence of the kink angle δ_K on the ratio K_1/K_3 for a droplet with strong perpendicular boundary conditions to the isotropic phase. Starting at $K_1/K_3=2$, kinks smoothly evolve by decreasing the kink angle from π to lower values.